Acta Agrobotanica

DOI: 10.5586/aa.1716

Publication history
Received: 2017-03-10
Accepted: 2017-05-15
Published: 2017-06-27

Handling editor
Bożena Denisow, Faculty of Horticulture and Landscape Architecture, University of Life Sciences in Lublin, Poland

Authors' contributions
MS and TR sectioned material for light microscopy; MS and BŁ did microscopic observations, digital documentation and its analysis; BŁ wrote the manuscript; PB grew plants and collected seeds; EZ sectioned material for transmission electron microscopy

Funding
This work was supported in part by MNiSW grant No. N N303 797240.

Competing interests
BŁ is an associate editor of the *Acta Agrobotanica*; other authors – no competing interests

Citation
Skawińska M, Łotocka B, Ruszkowski T, Banaszczak P, Znojek E. Root nodule structure in *Chamaecytisus podolicus*. Acta Agrobot. 2017;70(2):1716. https://doi.org/10.5586/aa.1716

ORIGINAL RESEARCH PAPER

Root nodule structure in *Chamaecytisus podolicus*

Monika Skawińska[1], Barbara Łotocka[1]*, Tomasz Ruszkowski[1], Piotr Banaszczak[2], Ewa Znojek[1]

[1] Department of Botany, Faculty of Agriculture and Biology, Warsaw University of Life Sciences – SGGW, Nowoursynowska 159, 02-776 Warsaw, Poland
[2] Arboretum, Warsaw University of Life Sciences – SGGW, Leśna 1, 95-063 Rogów, Poland

* Corresponding author. Email: barbara_lotocka@sggw.pl

Abstract
By means of microscopic analyses, it was shown that root nodules formed by *Chamaecytisus podolicus* exhibited all structural features typical for indeterminate nodules of temperate genistean shrubs: (***i***) apical nodule meristem composed of infected and non-infected domains, (***ii***) parenchymatous bacteroid-containing tissue with infected cells only resulting from mitotic activity of infected meristematic cells, (***iii***) absence of infection threads, and (***iv***) convoluted bacteroids singly enclosed in a symbiosome membrane. For the first time, it was shown that the nodule meristem is organized into longitudinal files of sister cells.

Keywords
indeterminate root nodule; root nodule meristem; endodermis; Genisteae; Fabaceae; bacteroid-containing tissue; symbiosome

Introduction

Chamaecytisus Link is regarded either as a monophyletic genus, morphologically uniform, or it is included into *Cytisus* Desf. sensu lato, section *Tubocytisus* DC [1]. As follows, *Ch. podolicus* (Błocki) A. Kláskova is also classified as *Cytisus podolicus* Błocki. In this work, the name *Ch. podolicus* is used by analogy with the genus taxonomy in the checklist of vascular plants of Poland [2].

Chamaecytisus podolicus (Fabaceae) is an endemic species of the Podolian Upland [1], mentioned in the red book of Ukraine as vulnerable [3]. The following brief species description is a compilation from a few sources [1,3,4]: xerophyte, calciclole, nanophanerophyte, stems ascending and hairy, leaves trifoliate with obovate pubescent leaflets, inflorescences (capitulum) terminal, each with 10–12 yellow flowers 25–30 mm long, primary bloom in June–July followed with a secondary one, calyx densely pubescent, standard 23–25 mm long, pods 25–30 mm long ripe in July–August.

The red book of Ukraine [3] as well as Ukrainian and Russian Internet sites related to commercial nursery and horticulture (e.g., [5]) indicate the economic and commercial value of *Ch. podolicus*, specifically as a decorative and melliferous plant. In Poland, the species is currently not known as a cultivated plant. However, this small shrub has grown very well in an alpine garden in the WULS Arboretum in Rogów, central Poland, since 1994, when it was introduced from seeds obtained from the UMCS Botanical Garden, and therefore seems worth both wider scientific investigation and recommending it to potential users.

Most fabacean species, especially in the Faboideae subfamily, form root nodules, which are organs specialized in controlled sustaining of rhizobia. Under symbiotic conditions, these soil bacteria reduce N^2 to NH_4^+ and provide it to the host plant. Root nodules are diverse as to their anatomy and ultrastructure, but generally they are classified into two types that differ in their meristematic persistence, viz, with the meristem of (***i***)

determinate or (***ii***) indeterminate growth [6]. Among genera that form indeterminate nodules, the genisteans (i.e., the tribe that includes *Chamaecytisus* spp.) seem distinct, with numerous unique developmental and structural features [7], the infected domain within the nodule meristem being the most important one. This work was undertaken to determine, on the basis of precise (ultra)structural observations, whether *Ch. podolicus* root nodules conform to the emerging genistean root nodule subtype.

Material and methods

For this work, seeds of *Ch. podolicus* were collected in 2010, from 16-year-old shrubs growing since ca. 1994 between limestone rocks in an alpine garden collection in the Arboretum in Rogów (Warsaw University of Life Sciences – SGGW), central Poland. Seeds were surface-sterilized and germinated as described earlier [8]. Seedlings were transferred to pots filled with sterile wet perlite and, after a few days, inoculated with rhizobia. Normally, plants would have been inoculated with rhizobia isolated from the same species. In this case, the root systems of "parent" plants were inaccessible for collection of root nodules and subsequent rhizobia isolation. However, it was observed earlier [8] that *Chamaecytisus* spp. plants are nodulated effectively with *Bradyrhizobium* strains isolated from the other genisteans. Therefore, a mixture of *Bradyrhizobium* strains Jan3, Jan8, Jan9, Jan14, Jan15 isolated from *Genista tinctoria* root nodule and WM9 from *Lupinus luteus* (all strains kindly provided by Prof. W. Małek, Marie Curie-Skłodowska University in Lublin) was used for seedling inoculation in this work.

Plants were grown under a 14 h light /10 h dark photoperiod at room temperature and supplemented daily with N-free medium described earlier [9]. Four weeks after inoculation, root nodules initiated within the oldest part of the root system were sampled for microscopy, fixed, post-fixed, dehydrated, and embedded in an epoxy resin as described earlier [8]. Ten nodules, each one taken from a different plant, were cut into semi-thin serial sections until the central sagittal section was obtained. Semi-thin sections, stained as described earlier [8], were used for anatomical analysis. Observations were done by means of a Provis AX70 (Olympus) light microscope and digital images were saved using a dedicated DP50 camera (Olympus) operating under AnalySIS software (SIS). Ultra-thin sections, prepared for observations as described earlier [8], were studied using a Morgagni 268D (FEI) transmission electron microscope (TEM). Images were saved using a Morada digital camera (SIS) operating under iTEM software (SIS).

Digital images were merged – if needed – using Photoshop CS6 (Adobe) software (panorama tool), and processed using the same software by means of non-destructive tools (contrast, levels, and/or curves). All adjustments were done in the whole area of the image. For every magnification used in Provis AX70, the image of linear micrometric scale was saved identically as described, to provide reference images for scale bars.

Analysis of cell lineages within the nodule meristem was done on central sections of the nodule meristem (non-central sections were not suitable) photographed at a resolution sufficient for the task. Using the Photoshop software, a new transparent layer was added to the original panorama image and cell walls at the boundary of cell lineages were drawn, taking into consideration, primarily, cell wall arrangement and thickness. When necessary, the cell arrangement was compared with the previous and next sections.

Results

Root nodules formed by *Ch. podolicus* were oblong or manifold-bifurcated at the time of sampling, and they were intensely pink on fresh section. Generally, the nodules were composed of apical persistent meristem, vascular system, and several specialized parenchymatous tissues, namely, the nodule cortical layers and the central bacteroid-containing tissue (Fig. 1a).

In the meristem of *Ch. podolicus* nodules, infected and non-infected cells were present within domains, which were clearly delimited (Fig. 1b,c, Fig. 2a–c), but symplastically

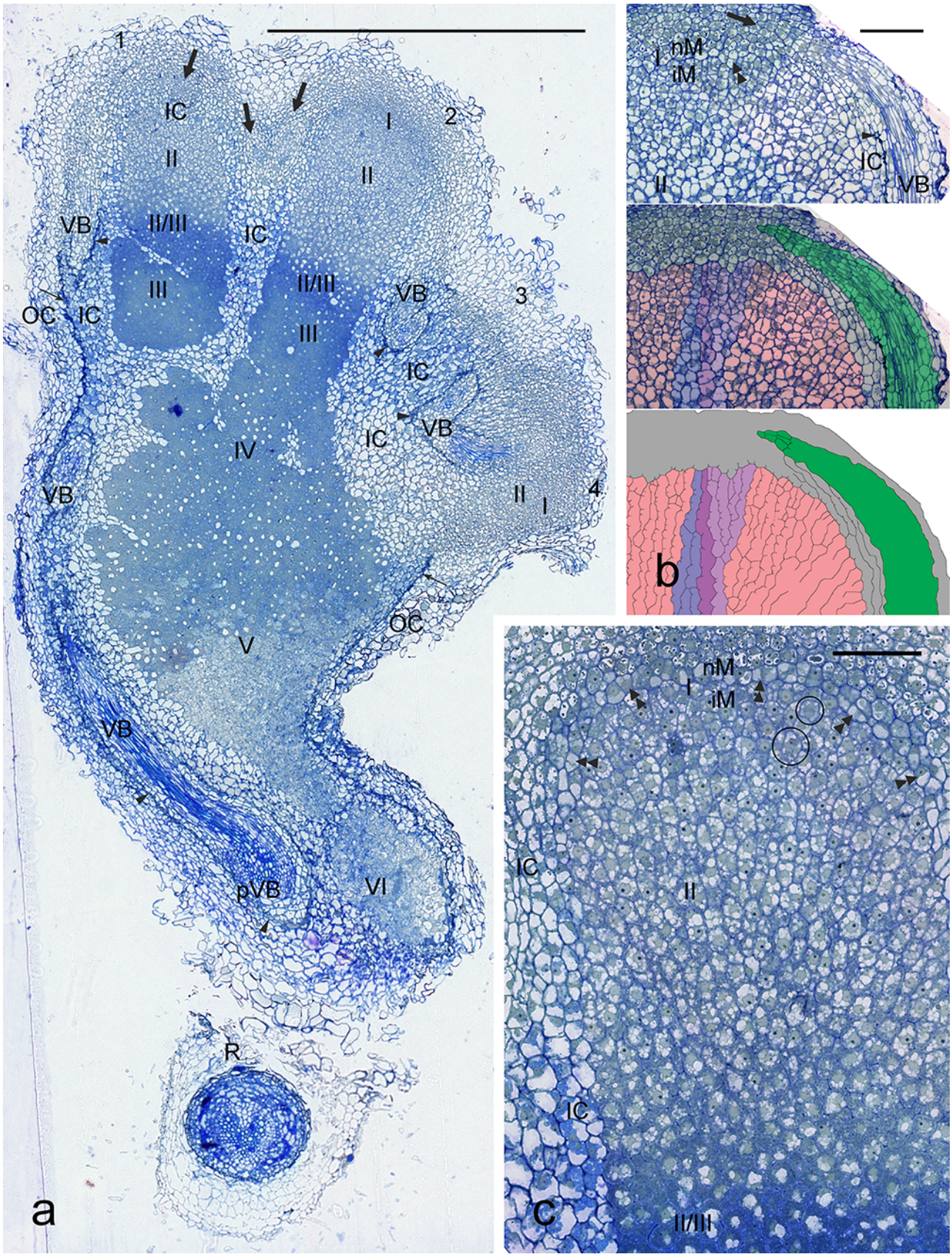
1
IC
II
VB
II/III
IC
III
OC
IC
II/III
III
VB
3
IC
IV
IC
VB
VB
II
I
4
OC
V
VB
pVB
VI
R
a
nM
I
iM
IC
II
VB
b
nM
I
iM
IC
II
IC
c
II/III

Fig. 1 The structure of *Chamaecytisus podolicus* root nodule, longitudinal sections. **a** General anatomy of root nodule. Scale bar = 1 mm. **b** Nodule meristem organization and cell lineages. Scale bar = 100 µm. **c** Magnification of the 2nd lobe from **a** on a distance from zone I (meristem) to II/III interzone; the section is not central, therefore the infected cell lineages are traceable on short distances only. Scale bar = 100 µm. 1, 2, 3, 4 – four lobes of the nodule, they are in different planes, therefore meristem is visible only in the 2nd and 4th lobe; I – meristematic zone; II – differentiation zone of the bacteroid-containing tissue (= early symbiotic zone); II/III – starch-rich interzone II/III; III – nitrogen-fixing (differentiated) zone; IV – senescent zone; V – degraded zone; VI – saprotrophic zone; IC – inner cortex of the nodule; thin arrows – nodule endodermis; OC – outer cortex; thick arrows – meristematic apices of vascular bundles; VB – vascular bundle; pVB – proximal vascular bundle; arrowheads – vascular endodermis; nM – non-infected domain of the nodule meristem; iM – infected domain of the meristem; double arrowheads – inner layer of the non-infected meristem domain, note that in **c** this layer is free of globular vacuolar deposits; circles – mitotic cells. Color codes: green – vascular bundle apex; grey – non-infected meristem domain and differentiating nodule cortex; pink – infected domain of the meristem and differentiating bacteroid-containing tissue, three cell lineages of contrasting history are marked with different shades (blue for a closing lineage, violet for constant one, and lilac for widening one).

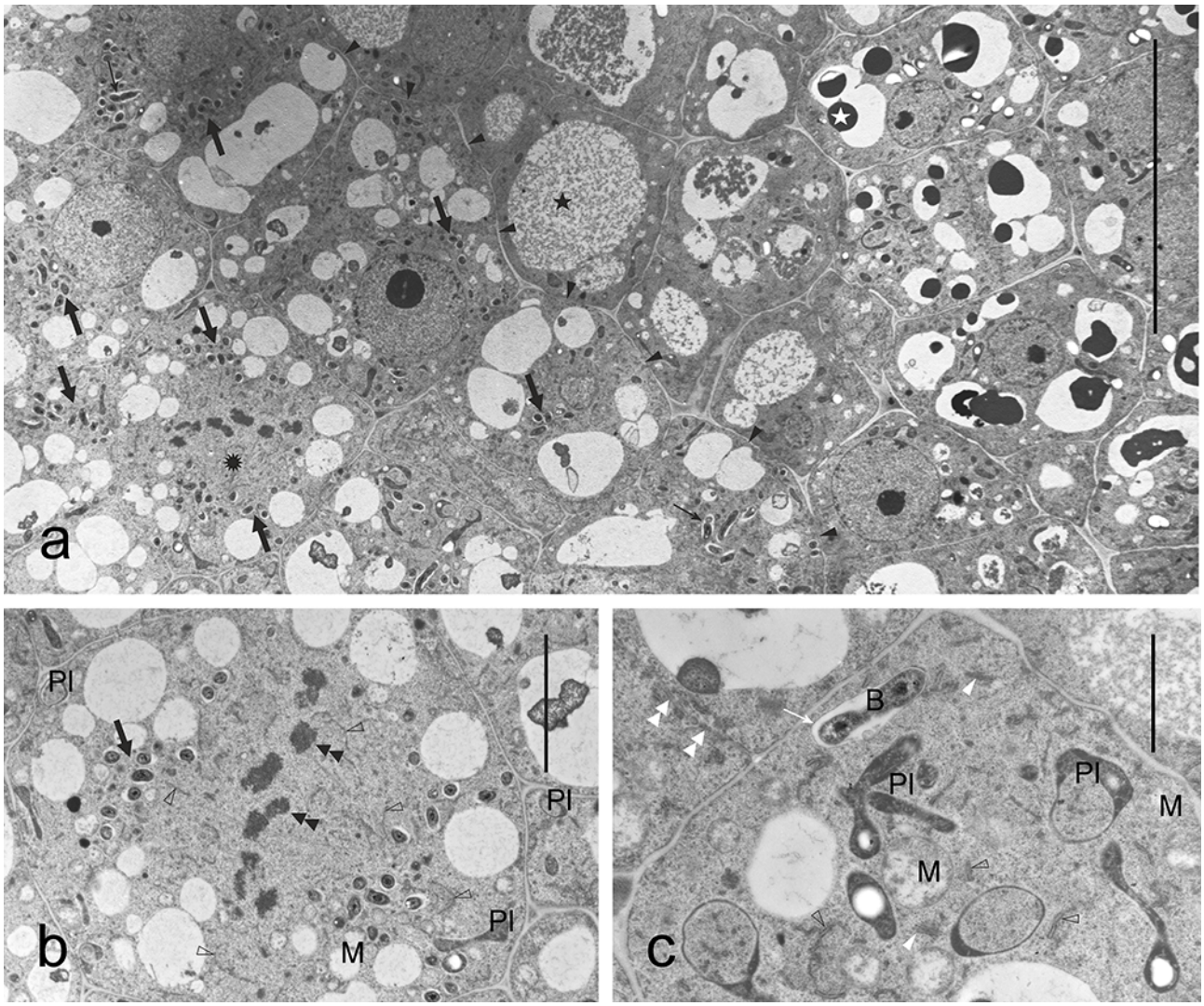

Fig. 2 The ultrastructure of nodule meristem in *Chamaecytisus podolicus*. **a** Boundary of infected and non-infected meristem domains. Scale bar = 20 µm. **b** Cell in metaphase, magnification from **a**. Scale bar = 5 µm. **c** Ultrastructure of infected meristematic cell. Scale bar = 2 µm. Arrowheads – cell walls at the boundary of non-infected and infected meristem domains; rosette – cell in metaphase; black asterisk – vacuolar fine deposits in the inner layer cells of non-infected domain; white asterisk – vacuolar electron-dense globules in the non-infected domain; slim arrows – symbiosomes with dividing bacteroid; thick arrows – symbiosomes; double arrowheads – chromosomes; open arrowhead – rough endoplasmic reticulum; Pl – plastids, note small starch grains and tubular tylakoid in **c**; M – mitochondria, note their electron-transparent matrix; B – bacteroid; white slim arrow – peribacteroid membrane; white arrowhead – dictyosome; double white arrowhead – cell plate in cytokinetic cell.

connected (not shown). Infected meristematic cells were proximally located vs. non-infected ones. Within the infected meristematic domain, transverse cell divisions prevailed, which resulted in the arrangement of sister cells into longitudinal files, as was revealed by means of the cell lineage analysis (Fig. 1b). The files of sister cells had various widths when traced through the whole distance between the proximal and distal boundaries of the infected domain: (***i***) constant, (***ii***) increasing, resulting from longitudinal divisions (reverse-T divisions), (***iii***) closing. At the distal end of widening files, the meristematic infected cells were smaller in comparison to the other files.

The most distal infected meristematic cells (i.e., the least differentiated) usually had just a few symbiosomes visible per section, and during mitosis these "hybrid organelles" were segregated similarly as the host's organelles (Fig. 2a,b). Among the latter, the most characteristic were short rough endoplasmic reticulum (RER) cisterns, concave plastids with the envelope's tubular invaginations, and mitochondria with electron-transparent matrix (Fig. 2c).

The non-infected meristematic cells were arranged into 3–4 layers of concave "covering" of the infected domain (Fig. 1b,c). In the non-infected domain, the inner 1–2 cell layers were distinctive, as they had fewer (or none) electron-dense globuli and anticlinal cell divisions prevailed in them. In the outer part of the non-infected domain, cells divided in different planes and rapidly differentiated into distal parenchyma. The cells of the non-infected domain produced lateral parts of the nodule – the nodule cortex (continuous with the mentioned distal parenchyma that covered and protected the meristem), together with provascular strands. The latter visibly tapered to a single cell within the lateral part of the non-infected domain (Fig. 1b).

At the proximal side of the infected domain, cells differentiated into parenchymatous bacteroid-containing tissue (termed also "bacteroid tissue") (Fig. 1a–c). The sole feature discriminating the proximal meristem from the distal differentiation zone were mitotic figures, therefore the transition was difficult to determine on section. Differentiating host cells became larger and more vacuolated. Their symbiosomes had wider peribacteroid space and elongated bacteroids, which in some symbiosomes divided transversely, as in the meristematic cells, with the division of peribacteroid membrane following. Within the nucleoid, electron-dense fibrils and granular polyphosphate inclusions were visible. Electron-transparent round "empty" spaces, interpreted as sites of poly-β-hydroxybutyrate storage, were small and sparse. The proliferation of RER occurred in the host's cells, and the cisterns were dispersed throughout the cytoplasm. At the proximal border of this zone, interzone II/III was formed: cell vacuolation decreased visibly, all mitochondria and plastids were positioned at cell walls facing intercellular spaces, and plastids contained several very large and flattened starch grains (Fig. 1a,c, Fig. 3b). In the interzone, symbiosomes had narrowed peribacteroid space and single bacteroids, which maintained an elongated shape but accumulated more poly-β-hydroxybutyrate (Fig. 3b).

In the differentiated bacteroid-containing tissue (= nitrogen-fixing zone), cells reached their maximal size. They had a single vacuole centrally located at the cell nucleus and abundant symbiosomes (Fig. 3a). Within the peribacteroid membrane, bacteroids were irregularly shaped, branched and/or convoluted (Fig. 4b).

In older bacteroid-containing tissue, senescence zone was formed (Fig. 1a, Fig. 5a). Degenerative changes were visible first in symbiosomes. The peribacteroid space widened and bacteroid cytoplasm became less electron-dense. Fusion of peribacteroid membranes with one another and with the tonoplast was evident (Fig. 5a). After degradation of bacteroids, remnants of their cell walls remained as the so-called "ghost membranes" (Fig. 5b,c). Concurrently, the host's compartment underwent complete degradation. Some of the resulting "empty" cells, devoid of living protoplasts or bacteroids, became populated by rod-shaped rhizobia that until now had survived within the bacteroid tissue in specialized apoplast enclaves (Fig. 4b). Such enclaves were rarely found in *Ch. podolicus* nodules. Thus, the saprotrophic zone (Fig. 1a, Fig. 5b) of the *Ch. podolicus* nodule was finally formed (it was initial in the nodules investigated), with cells filled with a fine-fibrillar matrix surrounding the rod-shaped rhizobia.

Within the whole extension of bacteroid-containing tissue, no infection threads were present. Also, non-infected cells were only occasionally found in this tissue and they were arranged in narrow longitudinal files.

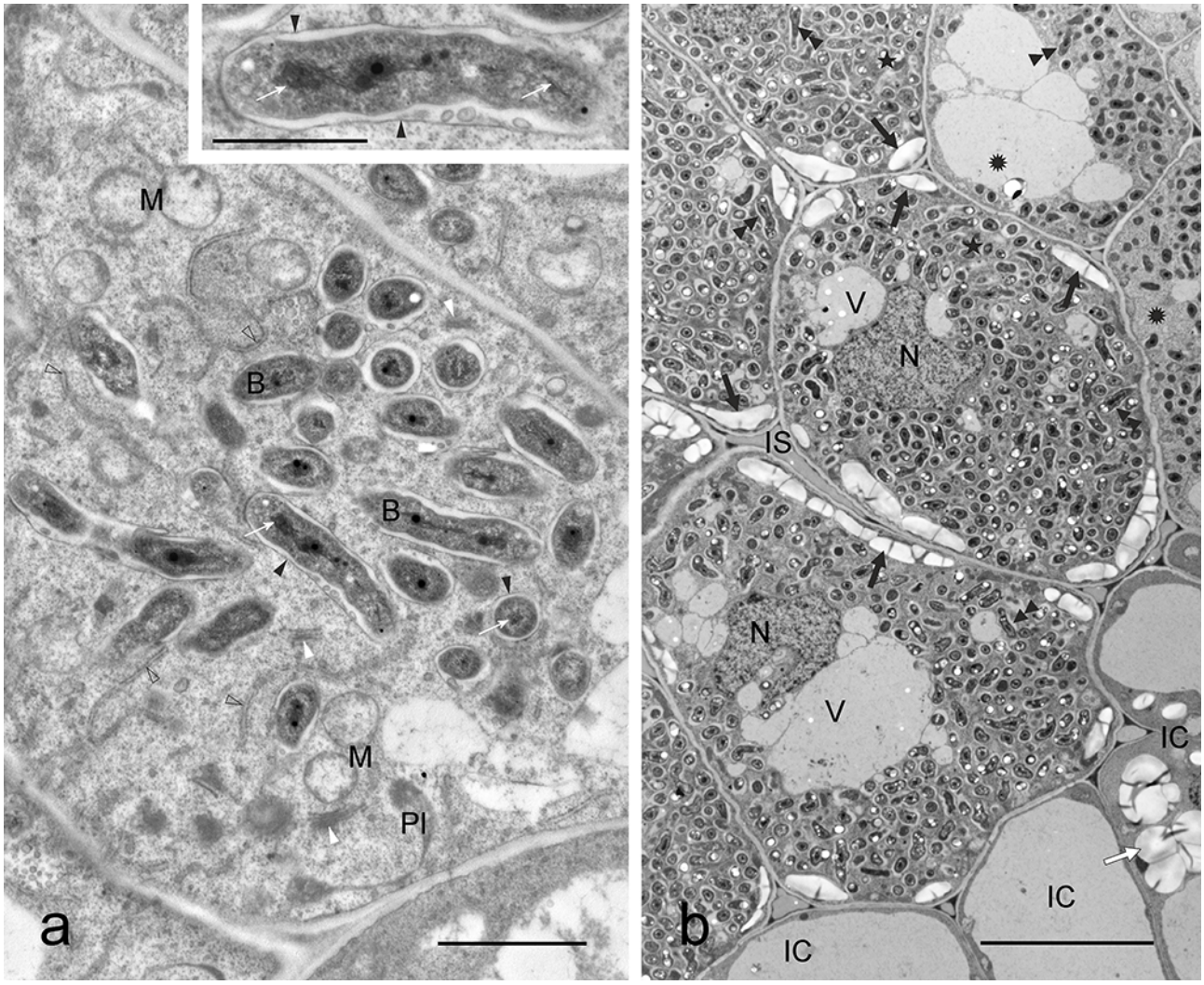

Fig. 3 The ultrastructure of differentiating cells of bacteroid-containing tissue in *Chamaecytisus podolicus* root nodule. **a** Early stage of differentiation, insert – symbiosome. Scale bars = 2 μm and 1 μm, respectively. **b** Boundary of pre-interzone and interzone II/III cells. Scale bar = 10 μm. Arrowheads – peribacteroid membrane (note vesicles within the peribacteroid space); white slim arrow – electron-dense, fibrillar nucleoid, note electron-dense globules in nucleoid shown in insert; white arrowheads – dictyosomes; open arrowheads – rough endoplasmic reticulum; rosettes – pre-interzone cells; asterisks – interzone II/III cells; black arrows – flat starch grains in bacteroid-containing cells; white arrow – rounded starch grains in inner cortex cells; double arrowheads – bacteroids longitudinally sectioned were elongated; B – bacteroid; Pl – plastids; M – mitochondria; IC – inner cortex; IS – intercellular space; N – nucleus; V – vacuole.

The bacteroid tissue of *Ch. podolicus* was laterally surrounded with three distinct layers of the nodule cortex (Fig. 1a). Within the thin parenchymatous outer cortex, cells were strongly vacuolated and they had few organelles. Large intercellular spaces were formed in this layer. The next tissue, the nodule endodermis (NE), was a single layer of flat cells devoid of the intercellular spaces leading to the inner cortex. With the exception of the nodule apex, NE was continuous within the nodule cortex and at the nodule base it was fused with the root endodermis. Cell walls of NE were thin and they contained a characteristically striated suberized layer (Fig. 6a). On this layer, the secondary cell wall was deposited that became lignified in older parts of the nodule. Often, the NE cells were not turgid and had folded walls. The inner cortex was parenchymatous, 4–6 cells thick. Two cell layers differentiated in this part. Facing NE, a layer occurred, which was a few cells deep and had characteristically folded anticlinal walls and fragmented or non-existent tonoplast (Fig. 6b). The cells adjoining bacteroid tissue, with their clearly defined tonoplast and large amyloplasts, were ultrastructurally distinct from the other inner cortex cells.

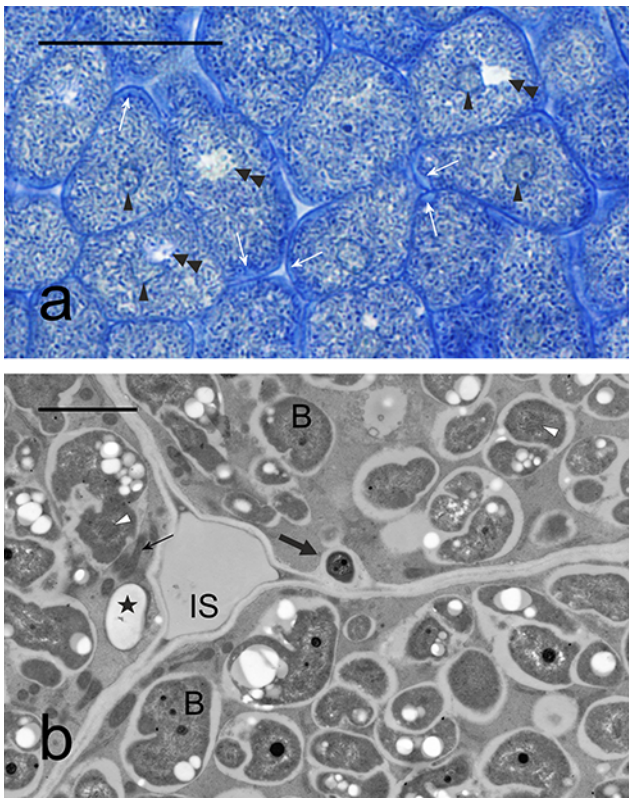

Fig. 4 The nitrogen-fixing (differentiated) zone cells of bacteroid-containing tissue in *Chamaecytisus podolicus* root nodule. **a** General structure. Scale bar = 50 µm. **b** Ultrastructure. Scale bar = 2 µm. Arrowheads – nuclei; double arrowheads – vacuole; white slim arrows – large amyloplasts located at intercellular spaces; black slim arrow – group of mitochondria; asterisk – starch grain; arrow – apoplastic enclave containing rhizobial cell; white arrowheads – nucleoids, note that their appearance was diffuse, with electron-dense globules; B – bacteroids with electron-transparent poly-beta-hydroxybutyrate grains, note irregular shape of bacteroids that can result in several profiles of the same bacteroid within single peribacteroid membrane; IS – intercellular space.

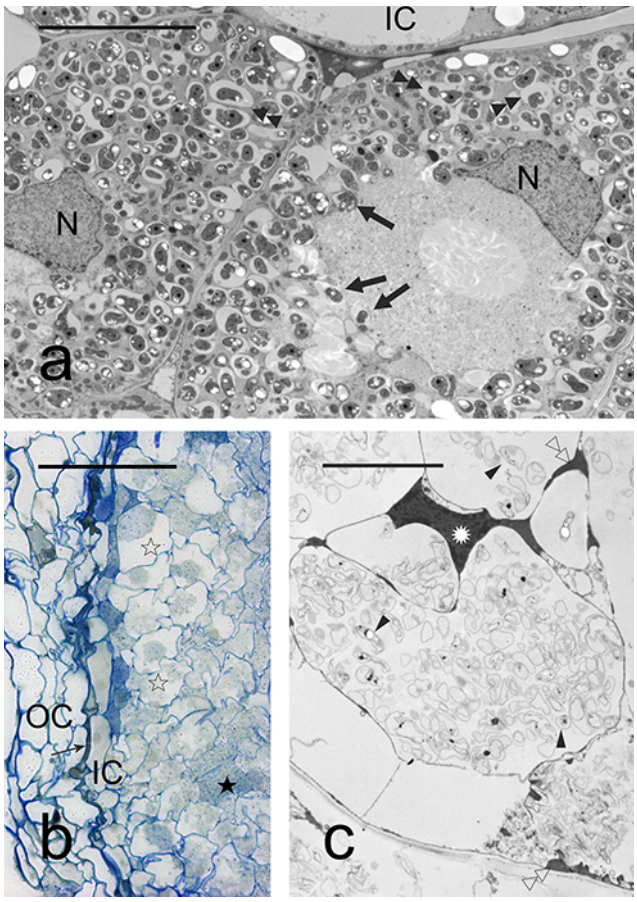

Fig. 5 The degradation of bacteroid-containing tissue in *Chamaecytisus podolicus* root nodule. **a** Infected cell degradation in the early senescent zone. Scale bar = 10 µm. **b** General structure of degraded/ saprotrophic zone. Scale bar = 100 µm. **c** Ultrastructure of the degraded cell. Scale bar = 5 µm. Arrows – inclusion of symbiosomes into the vacuole; double arrowheads – symbiosomes with widened peribacteroid space; IC – inner cortex cell; N – nucleus; OC – outer cortex, slim arrow – nodule endodermis, open asterisks – completely degraded cells with remnants of bacteroids; black asterisk – cell with a colony of saprotrophic rhizobia; rosette – degraded cell nucleus; open double arrowheads – remnants of host's cytoplasm and organelles; arrowheads – ghost membranes.

In *Ch. podolicus* nodules, vascular bundles were located at the boundary of inner cortex and nodule endodermis (Fig. 1a). Phloem and xylem were in diarch arrangement in most bundles (Fig. 7a), with occasional collateral arrangement (not shown). Phloem and xylem were surrounded with a layer, 2–3 cells deep, of parenchymatous pericycle and a single layer of vascular endodermis (Fig. 7a). Transfer cells were not found. At the nodule base, cortical bundles fused into a single basal one, which eventually merged with the root vascular tissues. In the basal bundle, vascular endodermis was in the 3rd developmental stage with a thick, striated, suberized layer and secondary cell wall (Fig. 7b,c), while it reached the 1st stage only (Casparian strip; not shown) in the vicinity of the young bacteroid-containing tissue.

Discussion

In the present work, plants of *Ch. podolicus* inoculated with a mix of genistean symbiotic rhizobia produced root nodules that were considered effective in dinitrogen fixation on the basis of deeply green color of the leaves. Also, fresh nodule sections

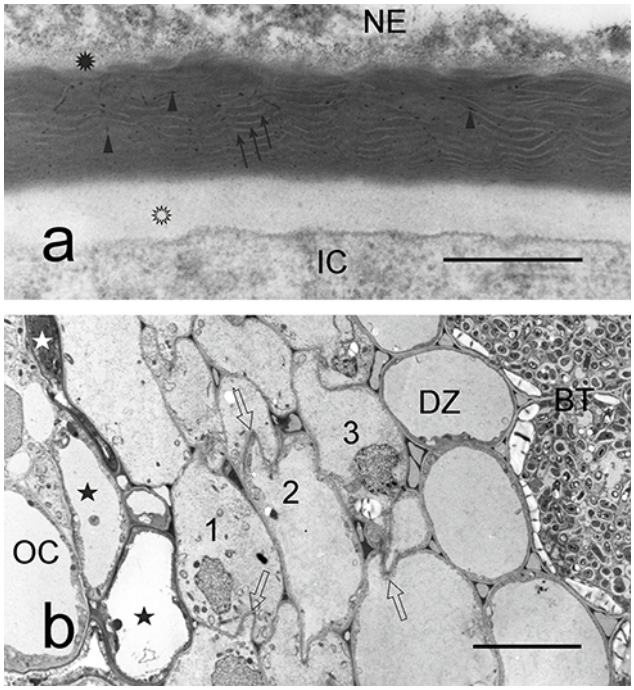

Fig. 6 The cortical tissues in *Chamaecytisus podolicus* root nodule. **a** Ultrastructure of the nodule endodermis cell wall. Scale bar = 0.5 µm. **b** Ultrastructure of inner cortex. Scale bar = 10 µm. Open rosette – cell wall of inner cortex (IC) cell; slim arrows – striated suberized layer; arrowheads – electron-dense deposits within suberized layer; black rosette – secondary cell wall of nodule endodermis (NE) cell (this layer becomes lignified); asterisks – NE cells; 1,2,3 – boundary layer, 3-cells wide here; open arrows – folded cell walls in non-turgid cells of boundary layer; DZ – distribution zone cells with intact vacuoles (boundary layer and DZ belong to inner cortex); BT – bacteroid-containing tissue; OC – outer cortex.

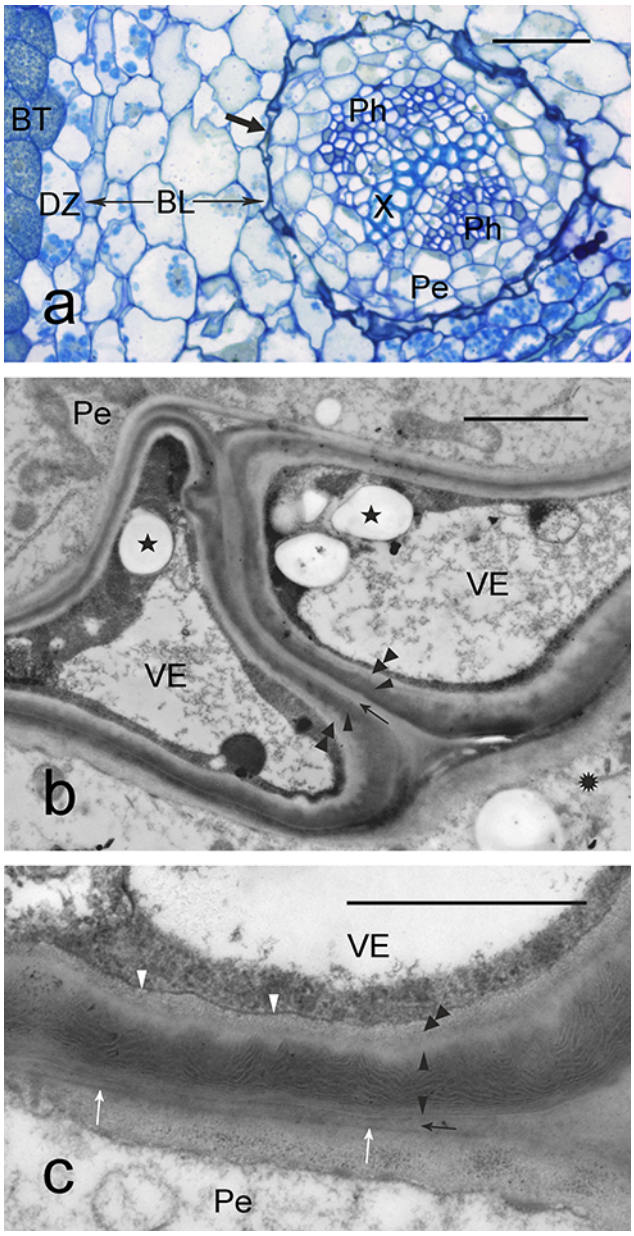

Fig. 7 The vascular bundles and vascular endodermis in *Chamaecytisus podolicus* root nodule. **a** General structure of proximal vascular bundle. Scale bar = 10 µm. **b** Ultrastructure of vascular endodermis in its 3rd developmental stage. Scale bar = 2 µm. **c** Ultrastructure of the cell wall in the 3rd stage vascular endodermis. Scale bar = 1 µm. Arrow – vascular endodermis, BT – bacteroid-containing tissue; DZ – distribution zone; BL – boundary layer; Pe – bundle pericycle; Ph – phloem; X – xylem; rosette – boundary layer cell; asterisks – starch grains; VE – vascular endodermis cells; white slim arrows – middle lamella between cell walls of VE and Pe cells; black slim arrow – primary cell wall of VE cell; black arrowheads – width of the striated suberized layer; double arrowhead – secondary cell wall of VE cell, this layer becomes lignified; white arrowheads – plasma membrane of VE cell.

were intensely pink, which is indicative of leghaemoglobin presence and, as follows, symbiosis functional in diazotrophy [6].

The structure of *Ch. podolicus* root nodules resembled, generally, the well-studied indeterminate nodules of *Trifolium* spp. [10], *Pisum sativum* [11], *Medicago sativa* [12], or model species *Medicago truncatula* [13], with their oblong shape, three distinct anatomical parts (nodule cortex, vascular system, and bacteroid-containing parenchyma) and longitudinal age-dependent zonation, most visible in bacteroid-containing tissue. However, significant differences, as compared to the mentioned species, were visible at the histological level. In the "classical" indeterminate nodules, the meristem is located apically and it consists of non-infected cells exclusively [14]. In the meristem of *Ch. podolicus* nodules, two domains were distinct, non-infected (distal) and infected (proximal). The domains differed also in the predominant cell division plane (anticlinal vs. transversal, respectively) and differentiation fates of the daughter cells, with the infected cells differentiating exclusively into bacteroid-containing parenchyma. Similar organization of the nodule meristem was previously described in cylindrical nodules of a few genistean shrubs: native to Poland *Genista tinctoria* [8], *Sarothamnus scoparius* [15], and *Ch. ratisbonensis* [7], or Mediterranean *Retama monosperma* [16] and *Ch. proliferus* [17]. Also, the cell ultrastructure (including coiled bacteroids within symbiosomes) of nodule tissues was similar between *Ch. podolicus* and the mentioned genisteans [7,8,15–17].

It is widely accepted that apical meristems are not subject to microbial infection (thanks to this phenomenon, infection-free plants are commercially produced from meristem explant by in vitro technologies [18: p. 232]). Generally, it is true, but some very interesting exceptions exist. For example, *Epichloë*/*Neotyphodium* fungal endophytes are vertically transmitted by caryopses of poacean hosts and, after germination, the seedling's aboveground organs become colonized by the endophyte intercellular growth from infected shoot apical meristem of the embryo [19]. Vertical transmission, via infected embryos, of an epiphytic obligatory bacterial symbiont occurs in certain rubiaceans and myrsinaceans [20,21]. Concerning root apical meristem, exceptions are not known (the query for "root apical meristem infection" or "RAM infection" yields zero results related to plants using Google Scholar search engine). The apical meristems of genistean root nodules described in the literature and in the present work are doubly exceptional regarding infection: they are formed within the root system, and the host's infection is intracellular. The question arises why the infected domain is strictly limited within the genistean nodule meristem: no cases of *Bradyrhizobium* sp. microsymbiont "escape" to the other part of the meristem are known to the authors, neither from the literature nor from personal experience. The answer may be simple: within the infected domain of the nodule meristem, rhizobial cells are enclosed with peribacteroid membrane. Having thus no access to the host cell wall, they cannot spread to the non-infected domain. Extrapolating from observations of rhizobial infection done on genistean *Lupinus luteus* [7,22], in the genistean/rhizobial symbiosis the events of rhizobial invasion via host cell wall penetration are restricted to just two stages: (***i***) the primary infection, e.g., the penetration of the root hair cell wall and, next, the cell wall separating the root hair cell base and the sub-rhizodermal nodule primordium cell, (***ii***) the rhizobia "escape" from apoplastic enclaves within the saprotrophic zone of the nodule. In both cases, rhizobial cells are in direct contact with the host cell wall surface, therefore, the enzymatic digestion of the host cell wall is possible, similar as was demonstrated in rhizobial infections occurring typically, e.g., with the formation of infection threads [23].

In this work, for the first time the non-random arrangement of cells was revealed within the *Ch. podolicus* nodule meristem, most evident within its infected domain. However, the arrangement of the files did not allow to identify clearly any "organization center" within the meristem, by analogy with root or shoot apical meristem. Rather, the mitotic activity was dispersed across the whole interface of infected and non-infected domains, possibly with higher frequency within the area of widening files, where the meristematic cells were smaller.

Interestingly, some of the longitudinal files of sister cells disappeared from the meristem, which may have resulted from the differentiation of the "founder cell" of the file. Such segmentation of the infected meristem was not proven earlier, although the examination of published images [7] suggests that it may be typical for oblong-shaped

root nodules of genisteans. It remains to be investigated whether it is a general rule in genisteans, as the anatomy of lupines' collar nodules is dissimilar [7].

In some *Ch. podolicus* nodules, an occasional file of non-infected cells was found within the infected domain, extending to a variable distance into differentiated bacteroid-containing tissue. Such file could have been formed due to asymmetrical segregation of symbiosomes during division of an infected cell and maintenance of mitoses in the resulting non-infected daughter cell.

In differentiating infected nodule cells, RER proliferation occurs, accompanying symbiosome multiplication, and in numerous fabaceans this process is associated with the formation of layered or coiled RER packets. In this study on *Ch. podolicus*, such RER arrangement was not observed, similarly as in *Ulex europaeus*, but in contrast to closely related *Ch. ratisbonensis* [7]. The interzone II/III, which constitutes the last stage of bacteroid-containing tissue differentiation, was for the first time described in *M. sativa* nodules [12], and it was shown that therein bacteroids reached the N_2-fixing stage, co-occurring with the expression of the host's leghaemoglobin. Since then, it was identified in all studies concerning the structure of indeterminate type nodules, including those formed by genistean species [7]. In this work, it was found also in *Ch. podolicus* nodules. In the differentiated bacteroid-containing tissue, both the host's cells as well as bacteroids reach their maximum size and mature shape. In *Ch. podolicus* nodules, bacteroids became irregular in shape and convoluted, and such bacteroids were deemed unique for temperate genisteans (excluding lupines) studied so far [7]. The process of saprotrophic zone formation also took a course typical for genisteans. In non-genistean indeterminate nodules, it is formed after complete degradation of infected cells and consists in the self-release of rod-stage rhizobia survived within the infection thread followed by their proliferation in the host's empty cells [24]. Such colonies gradually fill the cells, and the individual rods are embedded in a fine-fibrillar matrix. Since all bacteroids undergo degradation, only such rhizobia return to the soil after decomposition of the nodule. However, in genisteans described so far, a variant of the described process occurs, since in these plants infection threads are not formed during the whole organogenesis of the nodules [7]. Beginning with the nodule primordium formation, specialized enclaves containing rhizobial cells appear within the walls of non-differentiated infected cells, supposedly due to the (erroneous?) inclusion of a non-differentiated symbiosome into the new cell wall during cytokinesis. Such enclaves are unique for genisteans' root nodules. The enclaves remain apparently unchanged during cell differentiation, maturity, senescence, and degradation, and thereafter the wall delimiting them becomes discontinuous (probably digested) and rhizobia can escape the enclave and proliferate within the available space. Within *Ch. podolicus* studied herein, although the enclaves were very rare and small, they seemed sufficient to ensure the return of rhizobial population to the soil, since the colonies of saprotrophic rhizobia were developing in the basal portion of the examined nodules.

In contrast to the typical indeterminate-type nodules of *Trifolium* sp., *Pisum* sp., or *Medicago* sp., and in similarity to the described genistean indeterminate nodules [7], the bacteroid-containing tissue of *Ch. podolicus* was composed of infected cells with only occasional file of non-infected cells. It was suggested earlier that such inclusion of non-infected cells results from segregation of symbiosomes to single cell division pole in a cell located in the infected meristematic domain and subsequent divisions of such cell.

The structure of nodule cortex was typical in *Ch. podolicus*, including the presence of specialized layers. The nodule endodermis and the boundary layer had all the structural features described earlier as necessary for diminishing the inward diffusion of oxygen, an inhibitor of nitrogenase [25–27]. The cortical cells adjoining bacteroid tissue, ultrastructurally distinct, formed the distribution zone, as defined by Witty et al. [28]. The nodule vascular system was similar, considering both its architecture as well as ultrastructure, to that described earlier for temperate genisteans [7].

Conclusion

On the basis of microscopic observations of *Ch. podolicus* root nodules, the main structural features of these organs were identified as follows: (***i***) persistent nodule meristem located apically, (***ii***) division of meristem into two domains: infected and non-infected, (***iii***) bacteroid-containing tissue resulting from the mitotic activity of infected meristematic cells and the absence of infection threads, (***iv***) bacteroid tissue composed of infected cells, and (***v***) convoluted bacteroids singly enclosed in a symbiosome. All these features were earlier described in the root nodules of *S. scoparius* [15], *G. tinctoria* [8] as well as *U. europaeus* and *Ch. ratisbonensis* [7]. All the mentioned species are temperate shrubs and the nodule anatomy features listed are proposed here as symptomatic for this group of the Genisteae tribe.

References

1. Pifkó D, Shevera M. Proposal to conserve *Cytisus podolicus* (*Chamaecytisus podolicus*) against *Cytisus bucovinensis*, and *Cytisus blockianus* (*Chamaecytisus blockianus*) against *Cytisus kerneri* and *C. marilauni* (Leguminosae). Taxon. 2013;62:181–183.
2. Mirek Z, Piękoś-Mirkowa H, Zając A, Zając M, editors. Krytyczna lista roślin naczyniowych Polski [Internet]. Kraków: W. Szafer Institute of Botany, Polish Academy of Sciences. 2017 [cited 2017 Feb 20]. Available from: http://bomax.botany.pl/ib-db/check/
3. Chervona knyha Ukrayiny [Internet]. 2010–2017 [cited 2017 Feb 20]. Available from: http://redbook-ua.org/item/chamaecytisus-podolicus/
4. Tutin TG, Heywood VH, Burges NA, Moore DM, Valentine DH, Walters SM, et al., editors. Flora Europaea: Rosaceae to Umbelliferae; vol 2. London: Cambridge University Press; 1968.
5. Ènciklopediâ dekorativnyh sadovyh rastenij [Internet]. 2017 [cited 2017 Feb 20]. Available from: http://flower.onego.ru
6. Sprent JI. Nodulation in legumes. Kew: Royal Botanic Gardens; 2001.
7. Łotocka B. Anatomia rozwojowa i ultrastruktura brodawek korzeniowych o nieograniczonym wzroście i jej specyfika u roślin z plemienia Genisteae. Warszawa: Wydawnictwo SGGW; 2008. (Rozprawy Naukowe i Monografie).
8. Kalita M, Stępkowski T, Łotocka B, Małek W. Phylogeny and nodulation genes and symbiotic properties of *Genista tinctoria* bradyrhizobia. Arch Microbiol. 2006;186:87–97. https://doi.org/10.1007/s00203-006-0124-6
9. Łotocka B, Arciszewska-Kozubowska B, Dąbrowska K, Golinowski W. Growth analysis of root nodules in yellow lupin. Annals of the Warsaw University of Life Sciences – SGGW, Agriculture. 1995;29:3–12.
10. Łotocka B, Kopcińska J, Golinowski W. Morphogenesis of root nodules in white clover. I. Effective root nodules induced by the wild type of *Rhizobium leguminosarum* biovar. *trifolii*. Acta Soc Bot Pol. 1997;66:273–292. https://doi.org/10.5586/asbp.1997.032
11. Borucki W. Some new aspects of the pea (*Pisum sativum* L.) root nodule ultrastructure. Acta Soc Bot Pol. 1996;65:221–233. https://doi.org/10.5586/asbp.1996.035
12. Vasse J, de Billy F, Camut S, Truchet G. Correlation between ultrastructural differentiation of bacteroids and nitrogen fixation in alfalfa nodules. J Bacteriol. 1990;172:4295–4306. https://doi.org/10.1128/jb.172.8.4295-4306.1990
13. Xiao TT, Schilderink S, Moling S, Deinum EE, Kondorosi É, Franssen H, et al. Fate map of *Medicago truncatula* root nodules. Development. 2014;141:3517–3528. https://doi.org/10.1242/dev.110775
14. Łotocka B, Kopcińska J, Skalniak M. Review article: the meristem in indeterminate root nodules of Faboideae. Symbiosis. 2012;58:63–72. https://doi.org/10.1007/s13199-013-0225-3
15. Sajnaga E, Małek W, Łotocka B, Stępkowski T, Legocki AB. The root–nodule symbiosis between *Sarothamnus scoparius* L. and its microsymbionts. Antonie Van Leeuwenhoek. 2001;79:85–391. https://doi.org/10.1023/A:1012010328061

16. Selami N, Auriac MC, Catrice O, Capela D, Kaid-Harche M, Timmers T. Morphology and anatomy of root nodules of *Retama monosperma* (L.) Boiss. Plant Soil. 2014;379:109–119. https://doi.org/10.1007/s11104-014-2045-5
17. Vega-Hernández MC, Dazzo FB, Jarabo-Lorenzo A, Alfayate MC, León-Barrios M. Novel infection process in the indeterminate root nodule symbiosis between *Chamaecytisus proliferus* (tagasaste) and *Bradyrhizobium* sp. New Phytol. 2001;150:707–721. https://doi.org/10.1046/j.1469-8137.2001.00120.x
18. Trigiano RN, Gray DJ, editors. Plant tissue culture, development, and biotechnology. Boca Raton, FL: CRC Press; 2010.
19. Christensen MJ, Bennett RJ, Ansari HA, Koga H, Johnson RD, Bryan GT, et al. *Epichloë* endophytes grow by intercalary hyphal extension in elongating grass leaves. Fungal Genet Biol. 2008;45:84–93. https://doi.org/10.1016/j.fgb.2007.07.013
20. Bettelheim KA, Gordon JF, Taylor J. The detection of a strain of *Chromobacterium zividum* in the tissues of certain leaf-nodulated plants by the immunofluorescence technique. J Gen Microbiol. 1968;54:177–184. https://doi.org/10.1099/00221287-54-2-177
21. Lersten NR, Horner HTJ. Bacterial leaf nodule symbiosis in angiosperms with emphasis on Rubiaceae and Myrsinaceae. Bot Rev. 1976;42:145–214. https://doi.org/10.1007/BF02860721
22. Łotocka B, Kopcińska J, Górecka M, Golinowski W. Formation and abortion of root nodule primordia in *Lupinus luteus* L. Acta Biol Crac Ser Bot. 2000;42:87–102.
23. van Spronsen, PC, Bakhuizen R, van Brussel TAN, Kijne JW. Cell wall degradation during infection thread formation by the root nodule bacterium *Rhizobium leguminosarum* is a two-step process. Eur J Cell Biol. 1994;64:88–94.
24. Timmers ACJ, Soupéne E, Auriac MC, de Billy F, Vasse J, Boistard P, et al. Saprophytic intracellular rhizobia in alfalfa nodules. Molecular Plant–Microbe Interactions Journal. 2000;13:1204–1213. https://doi.org/10.1094/MPMI.2000.13.11.1204
25. Parsons R, Day DA. Mechanism of soybean nodule adaptation to different oxygen pressures. Plant Cell Environ. 1990;13:501–512. https://doi.org/10.1111/j.1365-3040.1990.tb01066.x
26. Brown SM, Walsh KB. Anatomy of the legume nodule cortex with respect to nodule permeability. Aust J Plant Physiol. 1994;21:49–68. https://doi.org/10.1071/PP9940049
27. Brown SM, Walsh KB. Anatomy of the legume nodule cortex: species survey of suberisation and intercellular glycoprotein. Aust J Plant Physiol. 1996;23:211–225. https://doi.org/10.1071/PP9960211
28. Witty JF, Skøt L, Revsbech NP. Direct evidence for changes in the resistance of legume root nodules to O_2 diffusion. J Exp Bot. 1987;38:1129–1140. https://doi.org/10.1093/jxb/38.7.1129

Struktura brodawek korzeniowych u *Chamaecytisus podolicus*

Streszczenie

Na podstawie analiz przeprowadzonych metodami mikroskopowymi wykazano, że brodawki korzeniowe powstające u *Chamecytisus podolicus* mają wszystkie cechy strukturalne typowe dla brodawek o nieograniczonym wzroście wytwarzanych przez krzewy klimatu umiarkowanego należące do plemienia Genisteae: (***i***) merystem apikalny składający się z domen zainfekowanej i niezainfekowanej, (***ii***) miękiszową tkankę bakteroidalną zawierającą tylko komórki zainfekowane, wytwarzaną poprzez podziały mitotyczne komórek zainfekowanych merystemu, (***iii***) brak nici infekcyjnych oraz (***iv***) zwinięte bakteroidy występujące pojedynczo w symbiosomach. Po raz pierwszy wykazano, że w merystemie brodawki występują podłużnie ułożone ciągi komórek siostrzanych.